The Journal of Physiology

Assessing the cardiac function from micro-gravity to hyper-gravity conditions through a validated multiscale modelling approach

Francesco Tripoli[1], Luca Ridolfi[2,3] and Stefania Scarsoglio[1,3]

[1] *Department of Mechanical and Aerospace Engineering, Politecnico di Torino, Turin, Italy*
[2] *Department of Environmental, Land and Infrastructure Engineering, Politecnico di Torino, Turin, Italy*
[3] *PolitoBioMed Lab, Politecnico di Torino, Turin, Italy*

Handling Editors: Bjorn Knollmann & Axel Loewe

The peer review history is available in the Supporting Information section of this article (https://doi.org/10.1113/JP287142#support-information-section).

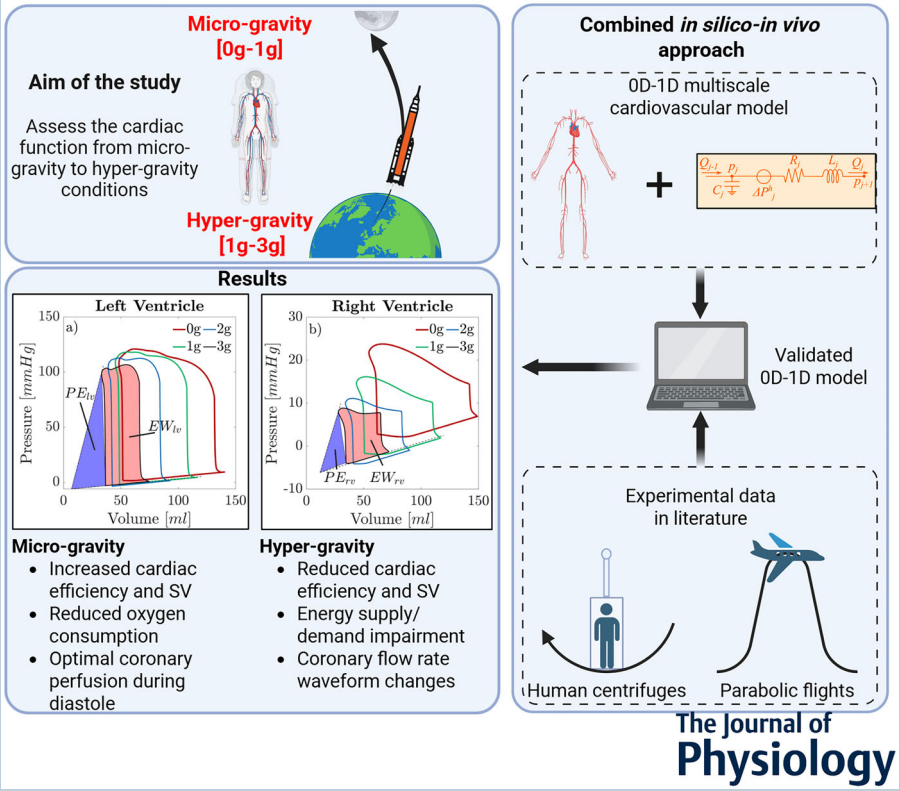

Abstract Figure Legend: Cardiac function in micro-gravity and hyper-gravity environments is still under investigation and restricted to a limited number of cardiac parameters. This study proposes to assess the cardiac function from micro- (0*g*) to hyper-gravity (3*g*) conditions through a multiscale modelling approach. The model has been validated using experimental data from literature (human centrifuge and parabolic flight studies). The model provides an in-depth description of the cardiac behaviour, revealing: (i) distinct responses between left and right heart haemodynamics (as shown by the left and right ventricular PV loops); (ii) enhanced cardiac efficiency and performance in micro-gravity; (iii) reduced cardiac efficiency along with impaired energy supply/demand ratio both at the heart and coronary levels in hyper-gravity.

 DOI: 10.1113/JP287142

Abstract Gravity changes with respect to the 1*g* terrestrial condition induce several cardiovascular alterations, from fluid shift and blood volume reduction to orthostatic hypotension and venous pooling. Micro-gravity and hyper-gravity exposure characterizes space missions and aeronautical flights, as well as terrestrial analogues such as centrifuges, bed rest studies, and parabolic flights. Despite a growing number of clinical measures becoming available, cardiac function in these extreme conditions is still incomplete and difficult to obtain. Thus, computational haemodynamics provides a powerful and reliable tool to understand the cardiac response. We propose a 0D-1D multiscale cardiovascular model to investigate the steady-state acute cardiac response to gravity changes (from 0*g* to 3*g*). The model combines a 1D description of the coronary circulation and arterial tree, with a 0D parameterization of the peripheral microcirculation, the venous return, the cardiopulmonary and the cerebrovascular-ocular circulations. The overall model is equipped with short-term regulation mechanisms, and accounts for gravity and posture changes. After a thorough validation using measured data from literature involving the most common central haemodynamic parameters (i.e. HR, MAP, SV and CO), the model provides an in-depth description of the cardiac response from micro- (0*g*) to hyper-gravity (3*g*), highlighting: (i) a different behaviour between left and right heart haemodynamics; (ii) an improvement in cardiac efficiency and cardiac performance in micro-gravity; (iii) a worsening of cardiac efficiency and an energy supply/demand impairment both at heart and coronary levels in hyper-gravity. Therefore, the modelling approach proves to be an important tool in shedding light on space medicine.

(Received 4 March 2025; accepted after revision 28 May 2025; first published online 26 June 2025)
Corresponding author S. Scarsoglio: Department of Mechanical and Aerospace Engineering, Politecnico di Torino, Corso Duca degli Abruzzi 24, Turin, 10129, Italy. Email: stefania.scarsoglio@polito.it

Key points

- Gravity changes from micro- to hyper-gravity induce several cardiovascular alterations, from fluid shift and blood volume reduction to orthostatic hypotension and venous pooling.
- Although the overall cardiovascular response is clear, details of the cardiac function in these extreme conditions are still incomplete and difficult to obtain.
- We propose a validated multiscale cardiovascular model to investigate the steady-state acute cardiac response to gravity changes (from 0*g* to 3*g*).
- After a thorough validation against the most common central haemodynamic parameters in literature, present results show: (i) a different behaviour between left and right heart haemodynamics; (ii) an improvement of cardiac efficiency and cardiac performance in micro-gravity; (iii) an energy supply/demand impairment in hyper-gravity.
- The computational approach is a useful and reliable tool in exploring the response of cardiac parameters which are difficult to investigate experimentally, aiming to shed light on the cardiac function under altered gravitational force.

Francesco Tripoli is a PhD student in Aerospace Engineering at Politecnico di Torino. He completed his MSc in Biomedical Engineering at Politecnico di Torino in 2022. From October 2022 to October 2023, he received a post-graduate research scholarship at Politecnico di Torino. During this period, he applied numerical methods to investigate cerebral haemodynamics in atrial fibrillation. His current research focuses on both cardiovascular and cerebro-ocular functions under spaceflight conditions, exploiting mathematical multiscale modelling. His work aims to enhance understanding of cardiovascular and cerebral deconditioning during long-term human spaceflight and to support the identification of effective countermeasure strategies.

Introduction

One of the most challenging issues of human space exploration and aeronautical flights is the exposure of the human body to gravitational force changes. During spaceflights, astronauts experience a wide range of gravitational accelerations (g), from weightlessness to increased gravitational stress sustained during launch or re-entry/landing manoeuvres. In addition, many terrestrial activities, from civil and military flights to skydiving or rollercoasters, expose the human body to varying levels of gravitational force. Changes in gravitational acceleration induce a number of physiological adaptations affecting musculoskeletal, cardiovascular and neurovestibular systems (Buckey, 2006; Clément, 2011; Young & Sutton, 2021). Understanding these adaptations is crucial to ensuring the health and safety of astronauts during future space missions and to developing effective countermeasures against deconditioning in the space environment (Hargens & Richardson, 2009; Hargens et al., 2013; Tanaka et al., 2017; Traon et al., 2007).

The cardiovascular system is greatly affected by gravitational acceleration, with deviations from terrestrial gravity eliciting a blood volume redistribution due to the gravity-dependent hydrostatic component of the blood pressure (Blomqvist & Stone, 1983). Despite the increasing number of studies on the cardiovascular response to gravity changes (Blaber et al., 2010; Hughson et al., 2018; Norsk, 2020; Shen & Frishman, 2019; Zhu et al., 2015), haemodynamic characterization is still incomplete and restricted to a limited number of cardiac parameters. Although the acquisition of clinical measures is difficult, it is thought that the micro-gravity-induced fluid shift from the lower to the upper body is the main driver of cardiovascular deconditioning (Hargens & Richardson, 2009; Norsk, 2020) – characterized by total blood volume reduction, cardiac atrophy and reduced exercise capability (Arbeille et al., 2001; Grigoriev et al., 2011; Zhu et al., 2015) – and spaceflight associated neuro-ocular syndrome (SANS) – characterized by several neuro-ocular anomalies triggered by elevated intracranial pressure (Berdahl et al., 2012; Taibbi et al., 2013; Zhang & Hargens, 2018). Conversely, hyper-gravity elicits a fluid shift in the cranio-caudal direction, exerting significant orthostatic stress on the cardiovascular system, which may result in reduced venous return to the heart and impaired cerebral perfusion (Blomqvist & Stone, 1983; Shender et al., 2003). Despite being a hazardous condition, some studies proposed that repetitive exposure to hyper-gravity may enhance tolerance to orthostatic stress, leading to adaptive cardiovascular responses (Convertino, 1998; Lalande & Buick, 2009; Newman & Callister, 2008; Newman et al., 1998), and that exposure to mild hyper-gravity may mitigate deconditioning induced by spaceflight hostile environment (Burton, 1988; Clément et al., 2015). Hence, understanding the cardiovascular response to micro- and hyper-gravity environments is critical for the implementation of countermeasures to protect astronauts during long-term spaceflight.

Ground-based analogues – such as bed-rest studies (Saveko et al., 2023; Traon et al., 2007), parabolic flights (Karmali & Shelhamer, 2008; Shelhamer, 2016) and human centrifuges (Goswami et al., 2015; Scott et al., 2007) – represent the easiest way to study the effect of gravitational acceleration changes in a controlled environment. However, these analogues have some limitations: (i) in bed-rest studies, the gravitational force (which typically acts on the longitudinal axis) is exerted on the antero-posterior axis, thus not eliminating the body weight; (ii) in human centrifuges, a gravity gradient along the longitudinal (head-feet) axis is produced due to the radius-dependent centrifugal force achieved by steady rotation; (iii) in parabolic flights, the real micro- and hyper-gravity environments are reproduced only for a few seconds (Karmali & Shelhamer, 2008). Moreover, the challenge of monitoring and recording detailed clinical data of the cardiovascular system – which is a complex issue even in controlled environment conditions due to the intrinsic limitations of the current acquisition methodologies – is amplified by several design constraints inherent in each analogue.

Mathematical modelling may represent a feasible tool to investigate the cardiovascular response to gravity alterations and clarify physiological aspects that are still unclear. A computational approach and, in particular, multiscale modelling allow distinct elements of the cardiovascular system to be described effectively, by combining sub-models with different levels of detail (from 0D to 3D models). Each compartment is able to reproduce the main haemodynamic features of a specific vascular region and different physiological mechanisms – such as short-term regulation mechanisms mediated by the autonomic system – can be implemented. Because of these properties, in recent years multiscale mathematical modelling has become a feasible method for investigating the haemodynamic response to different cardiovascular diseases – for example, cardiac arrhythmias and haemorrhages (Anselmino et al., 2016; Canuto et al., 2018; Saglietto et al., 2024) – and working conditions where gravitational acceleration plays a crucial role like head-up and head-down tilt tests and the human centrifuge (Diaz-Artiles et al., 2019; Fois, Maule, et al., 2022; Fois et al., 2024; Heldt et al., 2002; Whittle & Diaz-Artiles, 2021).

In this work, by exploiting a multiscale 0D-1D cardiovascular model, we describe the cardiac function in standing posture across a broad spectrum of gravity intensity: from micro-gravity (0g) to hyper-gravity (3g).

In particular, the steady-state acute response – which is mediated by short-term regulation mechanisms and occurs within few minutes following the application of an external stimulus – is investigated. The model includes a 0D–1D modelling of the systemic and coronary circulation, a 0D model of the cerebrovascular circulation, and has been recently validated and used to investigate cardiovascular and cerebro-ocular haemodynamics against different ground-based and spaceflight applications (Fois, Maule, et al., 2022; Fois, Ridolfi, et al., 2022; Fois et al., 2024; Gallo et al., 2020).

After an in-depth validation through existing literature involving the most common central haemodynamic parameters, we study the cardiac response from micro- (0*g*) to hyper-gravity (3*g*) by focusing on: left and right heart haemodynamics (including central venous and pulmonary capillary wedge pressures), left and right coronary circulation (left anterior descending artery and right coronary artery), pulmonary artery pressure, and indexes of oxygen consumption, cardiac work and efficiency.

Methods

Mathematical modelling

The mathematical framework employed in this work is based on a closed-loop 0D–1D multiscale model of the entire cardiovascular system (Fois et al., 2024). An overview of the model architecture is illustrated in Fig. 1. The cardiovascular model comprises a 1D description of the arterial tree along with the main coronary arteries and a 0D representation of the peripheral, venous, cardio-pulmonary, coronary and cerebro-ocular circulations. In this section, a brief description of the model structure and the implemented physiological features is given, whereas additional numerical details, including equations and parameter settings, are reported in our previous work (Fois et al., 2024) and are available through the link in the Additional Information section (please refer to the Supporting Information file).

The 1D arterial tree (left side of Fig. 1) consists of 48 main large arteries (from the ascending aorta to upper and lower limbs arteries) and 15 coronary arteries, for a total of 63 vessels. Each artery is modelled as a straight tapered vessel with a circular cross-section. Blood is modelled as an incompressible and Newtonian fluid with constant density $\rho = 1050$ kg/m^3 and viscosity $\mu = 4 \times 10^{-3}$ Pa s. These hypotheses permit the description of blood motion through the 1D axisymmetric form of the Navier-Stokes equations, taking the lumen area $A(x,t)$ and the blood flow rate $Q(x,t)$ as dependent variables (x is the axial vessel coordinate, and t is the time). To close the 1D mathematical system and to model the viscoelastic mechanical properties of the large artery walls, a non-linear constitutive equation associating the arterial blood pressure $p(x,t)$ with $A(x,t)$ is introduced (Fois et al., 2024). The model accounts for the gravity force by explicitly including a properly orientated gravitational term in the momentum balance equation. At each arterial bifurcation, the conservation of mass and total pressure is imposed as a boundary condition.

The inlet of the 1D ascending aorta is linked with the 0D aortic valve model, and each of the 24 1D terminal arteries is coupled by means of a characteristic impedance Z_c with a three-element *RLC* Windkessel model of the 0D arteriolar compartment. Each boundary value problem is treated by applying the method of characteristics (Fois et al., 2024). The 1D governing equations are solved numerically using the Discontinuous Galerkin Finite Elements method combined with a 2-step Runge-Kutta explicit time integration scheme.

The 0D model of the peripheral and venous circulations is characterized by several interconnected three-element *RLC* Windkessel models, with R, L and C describing the hydraulic resistance, the blood inertia, and the compliance of a specific 0D compartment, respectively. Specifically, arteriolar compartments merge into five body regions: extracranial circulation, arms, upper abdomen, lower abdomen and legs. Each of these regions comprises a capillary, venular and venous district. Three additional districts, describing the superior, inferior and abdominal segments of the vena cava, connect the venous compartments with the right atrium, thus closing the systemic circulation and completing the venous return to the heart. For each compartment, the governing equations are written in terms of the flow rate $Q(t)$, the blood volume $V(t)$, and the intraluminal pressure $p(t)$. For legs venous and superior vena cava districts, two different non-linear pressure-volume relationships are implemented to model the non-linear effects of distending leg veins volume (Fois et al., 2024) and venous collapse of neck veins (Holmlund et al., 2018; Lu et al., 2001). Additionally, arm and leg venous compartments are provided with a 0D model of venous valves. To insert the gravity contribution, a pressure generator is added in the venous and vena cava compartments according to Stevino's law.

The 0D model of the cardio-pulmonary circulation combines four 0D models, each describing a specific cardiac chamber, with a 0D model of the pulmonary circulation. To model the contraction of atria and ventricles a time-varying elastance is employed, whereas to model cardiac valves non-ideal diodes are used. Moreover, intrathoracic pressure (ITP), which depends on both gravity and body position (Fois, Maule, et al., 2022), acts as extravascular pressure, affecting the behaviour of all compartments of the cardio-pulmonary circulation.

The cerebro-ocular circulation is connected with the systemic arterial circulation via the internal

carotid and the vertebral arteries, whereas the venous outflow is directly connected to the superior vena cava compartment. The cerebral model (Fois et al., 2024) describes the cerebral blood flow within the large cerebral arteries, the circle of Willis and the distal cerebral circulation. Furthermore, it models the cerebrospinal dynamics and estimates the intracranial pressure (ICP) by imposing the mass conservation and assuming a non-linear intracranial compliance. The 0D model of the eye (Fois et al., 2024) includes six ocular compartments and is able to reproduce both intraocular pressure (IOP) and ocular globe volume.

The whole cardiovascular model is equipped with short-term autonomic control mechanisms, simulating the baroreflex and the cardio-pulmonary reflex (Fois et al., 2024). For both reflexes, sympathetic and parasympathetic activities are governed by two sigmoid functions (which depend on the mean aortic-carotid sinus pressure for the baroreflex, and the central venous pressure for the cardiopulmonary reflex). The baroreflex model regulates both peripheral resistances and venous tone and exerts an inotropic and chronotropic effect on both ventricles, whereas the cardiopulmonary reflex accounts only for peripheral vascular adjustments. Additionally, the 0D cerebral model accounts for the cerebral auto-regulation mechanism by changing the compliances and the hydraulic resistances of the distal cerebral circulation. The implementation of these regulation mechanisms

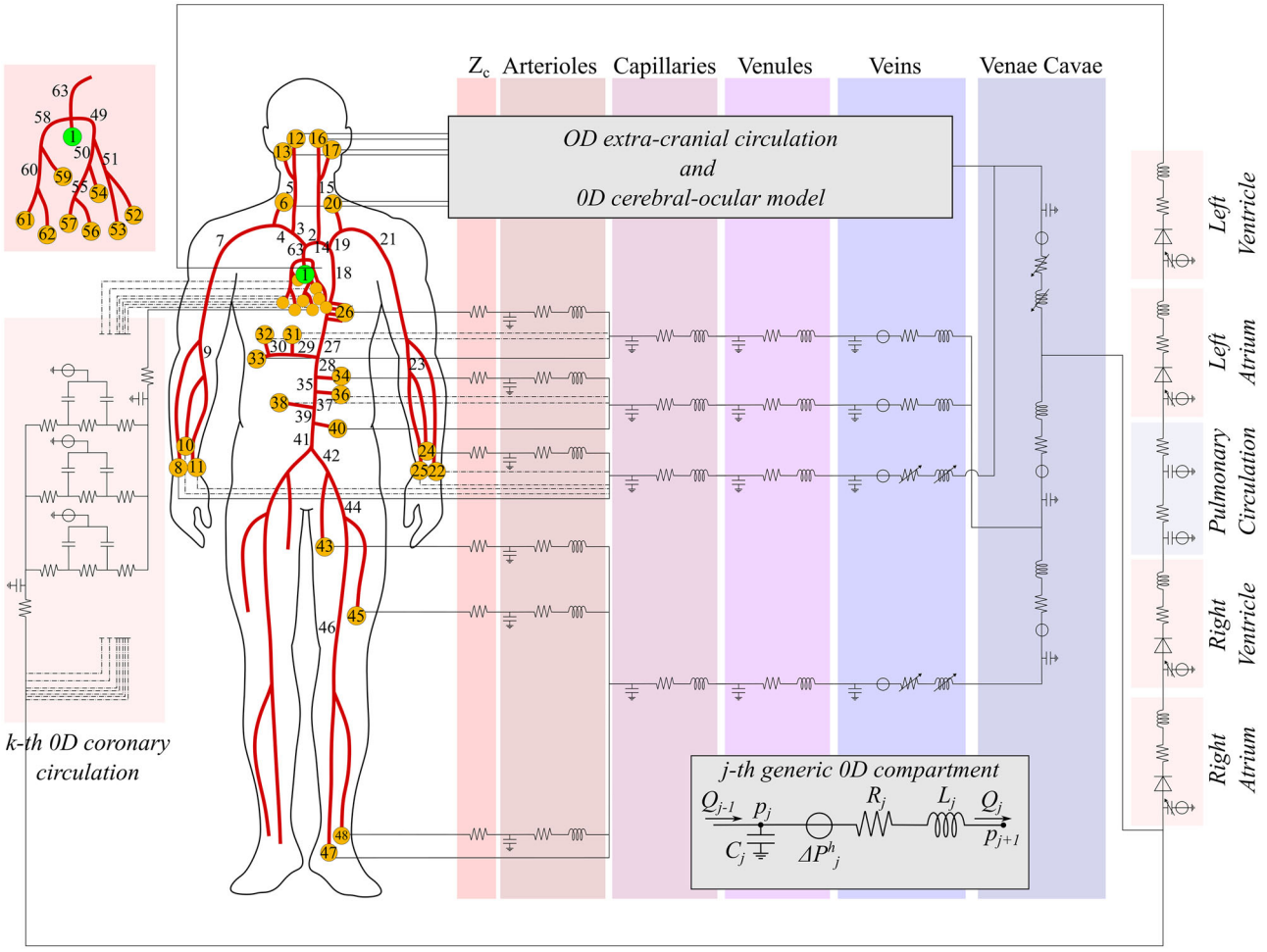

Figure 1. Schematic representation of the closed-loop 0D-1D multiscale model of the cardiovascular system
On the left, the 1D arterial tree is depicted in red, with numbers, and yellow and green circles indicating the specific arterial vessel, the outlets and the inlet of the 1D arterial tree, respectively. On the right, a representation of the 0D peripheral circulation, which is organized into five body regions (extracranial circulation, arms, upper abdomen, lower abdomen, and legs), is shown. Vertical rectangles refer to arteriolar, capillary, venular, venous and venae cavae compartments. The *k-th* generic 0D coronary microvascular region is depicted in the left box, the boxes on the right represent the cardio-pulmonary circulation, whereas the grey box at the bottom shows the *j-th* generic 0D compartment: Q_j is the flow rate, p_j is the pressure, Δp_j^h is the hydrostatic gradient, and R_j, C_j and L_j are compartmental resistance, compliance and inertance, respectively).

allows the model to simulate the short-term response to both posture and gravity changes.

To obtain the steady-state cardiovascular response in a standing posture, we first simulated a head-up tilt test at 1*g*. In this first step, the time dependence of the tilt angle α was computed as:

$$\alpha(t) = \begin{cases} 0 & \text{if } t < t^I_{\text{start}} \\ \frac{\alpha_{\text{tilt}}}{2} \cdot \left[1 - \cos\left(\frac{t - t^I_{\text{start}}}{T_{\text{tilt}}} \cdot \pi\right)\right] & \text{if } t^I_{\text{start}} < t < t^I_{\text{start}} + T_{\text{tilt}} \\ \alpha_{\text{tilt}} & \text{if } t > t^I_{\text{start}} + T_{\text{tilt}}, \end{cases} \quad (1)$$

where α_{tilt} represents the angle reached after the tilt (90°), t^I_{start} indicates the tilting starting time, and T_{tilt} denotes the tilting period in which the posture change occurred (22.5 s), respectively. Subsequently, starting from the standing 1*g* steady-state condition, gravity transitions from 1*g* up to the desired level of gravity were imposed by the cosinusoidal function:

$$\frac{g(t)}{g_0} = \begin{cases} 1 & \text{if } t < t^{II}_{\text{start}} \\ 1 + \frac{1}{2}\left[\left(\frac{g}{g_0}\right)_f - 1\right] \cdot \left[1 - \cos\left(\frac{t - t^{II}_{\text{start}}}{T_g} \cdot \pi\right)\right] & \text{if } t^{\text{start}}_{II} < t < t^{\text{start}}_{II} + T_g \\ \left(\frac{g}{g_0}\right)_f & \text{if } t > t^{II}_{\text{start}} + T_g, \end{cases} \quad (2)$$

where $(\frac{g}{g_0})_f$, t^{II}_{start}, and T_g indicate the final gravity level reached after the transition, the transition starting time, and the transition duration, respectively. To simulate both posture and gravity changes, t_{start} was selected in order to ensure that the initial transient resulting from model initialization was fully extinguished. Additionally, to prevent numerical instabilities, in particular at higher *g* values, all simulations were performed with a fixed gravity rate of ±0.01 g/s. While this gravity rate may not reflect typical real-life applications, our study is focused on the short-term steady-state condition, which is independent of the gravity rate (Fois, Maule, et al., 2022). A total of 31 simulations were conducted with *g* varying in the range [0*g*–3*g*].

Cardiac and coronary haemodynamic parameters

We here introduce the haemodynamic parameters used to describe the cardiac and coronary responses to gravity changes in the Results section. To assess the cardiac function, we focus our attention on the main mechano-energetic and efficiency indexes of the left and right ventricles. In particular, starting from each ventricle pressure-volume loop (PV loop) (see Fig. 3), it is possible to define the external work $\text{EW}_{lv/rv}$ (J) as the area of left/right PV loop, and the potential energy $\text{PE}_{lv/rv}$ (J) as the area of the triangles depicted in Fig. 3*A* and *B* (Westerhof et al., 2019). An additional mechano-energetic parameter, which can be derived from $\text{EW}_{lv/rv}$ and $\text{PE}_{lv/rv}$, is the left/right ventricle pressure-volume area, $\text{PVA}_{lv/rv}$ (J), defined as:

$$\text{PVA}_{\text{lv/rv}} = \text{EW}_{\text{lv/rv}} + \text{PE}_{\text{lv/rv}}. \quad (3)$$

With regard to cardiac efficiency, left/right ventricular efficiency (LVE and RVE) and ejection fraction ($\text{EF}_{lv/rv}$) are considered:

$$\text{LVE } (or \text{ RVE}) = \frac{\text{EW}_{\text{lv/rv}}}{\text{PVA}_{\text{lv/rv}}}, \quad (4)$$

$$\text{EF}_{\text{lv/rv}} = \frac{\text{SV}_{\text{lv/rv}}}{\text{EDV}_{\text{lv/rv}}}, \quad (5)$$

where $\text{SV}_{\text{lv/rv}} = \text{EDV}_{\text{lv/rv}} - \text{ESV}_{\text{lv/rv}}$ is the stroke volume (ml), that is the blood volume ejected from the left/right ventricle during a single cardiac cycle, $\text{EDV}_{\text{lv/rv}}$ (ml) is the left/right ventricle end-diastolic volume (defined by the closure of the mitral/tricuspid valve), and $\text{ESV}_{\text{lv/rv}}$ (ml) is the the left/right ventricle end-systolic volume (defined by the closure of the aortic/pulmonary valve).

In the literature, the most common methods to assess the cardiac oxygen consumption indexes, which are mainly based on pressure and heart rate, are the rate-pressure product (RPP (mmHg/min)) and the tension-time index (TTI (mmHg·s)), both defined as (Westerhof et al., 2019):

$$\text{RPP} = P_{\text{aa,sys}} \cdot \text{HR}, \quad (6)$$

$$\text{TTI} = P_{\text{lv,mean}} \cdot \text{RR}, \quad (7)$$

where $P_{aa,sys}$, $P_{lv,mean}$, HR and RR are the aortic systolic pressure, the mean left ventricle pressure, the heart rate and the cardiac cycle duration (HR = 60/RR), respectively. In this study, since we are interested in the cardiac work and oxygen consumption expressed per minute, these mechano-energetic and oxygen consumption indexes, apart from RPP, are multiplied by HR (i.e. $EW_{lv/rv}$/min (J/min), $PE_{lv/rv}$/min (J/min), $PVA_{lv/rv}$/min (J/min), and TTI/min (mmHg·s/min)).

To assess coronary perfusion at different levels of gravitational acceleration, two of the main branches of coronary circulation are investigated. Specifically, blood flows in the left anterior descending artery (LAD) – which is a branch of the left coronary artery and supplies blood to the anterior region of the left ventricle – and the right coronary artery (RCA) – which originates from the right aortic sinus and supplies blood to both the right ventricle and atrium – are evaluated. The analysed haemodynamic parameters are the coronary stroke volume ($SV_{LAD/RCA}$ (ml)), the coronary blood flow ($CBF_{LAD/RCA}$ (ml/min)), and the coronary perfusion pressure ($CPP_{LAD/RCA}$ (mmHg)), which are respectively defined as follows:

$$\begin{aligned} SV_{LAD/RCA} &= SV_{sys,LAD/RCA} + SV_{dia,LAD/RCA} = \\ &= \int_{RR_{sys}} Q_{LAD/RCA}(t) \cdot dt + \int_{RR_{dia}} Q_{LAD/RCA}(t) \cdot dt, \end{aligned} \quad (8)$$

where RR_{sys}, RR_{dia} are the systolic and diastolic intervals, and $Q_{LAD/RCA}$ is the flow rate within the LAD/RCA artery; and

$$CBF_{LAD/RCA} = SV_{LAD/RCA} \cdot HR, \quad (9)$$

$$CPP_{LAD/RCA} = P_{aa,dia} - EDP_{lv/rv}, \quad (10)$$

with $P_{aa,dia}$ being the diastolic aortic pressure.

Model validation

The existing literature provides very limited data on short-term cardiac response to actual spaceflight conditions of micro- and hyper-gravity. In particular, the haemodynamic parameters associated with the right heart, along with metrics for oxygen consumption, and coronary and cerebro-ocular circulations are poorly understood in both micro- and hyper-gravity environments. To validate our model, we relied on experimental measurements extracted from parabolic flight and centrifuge studies (Diaz-Artiles et al., 2018; Fontolliet et al., 2015; Habazettl et al., 2016; Konishi et al., 2019; Ogawa et al., 2016; Ueda et al., 2015) (please, refer to the link in the Additional Information section for raw data about the validation dataset constructed from experimental measures extracted from the literature). In order to enlarge the validation dataset, parabolic flight campaigns assessing both standing (Caiani et al., 2006, 2007; Lathers et al., 1989; Liu et al., 2012; Mukai et al., 1991) and sitting postures (Beckers et al., 2003; Klein et al., 2019; Norsk et al., 1987, 2006; Ogoh et al., 2015; Petersen et al., 2011; Pump et al., 1999; Widjaja et al., 2015) were included. Parabolic flights expose the cardiovascular system to a sequence of hyper-gravity and micro-gravity phases, each lasting only a few seconds, during which accelerations of 1.8*g* and 0*g* are typically reached. Human centrifuge studies achieve higher *g* forces, thereby allowing us to extend the validation dataset to the gravity range [0*g*–2.5*g*]. However, it should be noted that, as happens in real space- and aeronautical flight conditions, our model correctly reproduces a uniform gravitational acceleration along the longitudinal axis, whereas centrifuge-induced hyper-gravity entails a gravity acceleration gradient along the head-feet axis (or *z*-axis). Moreover, in the considered experimental datasets the radius of the centrifuge varied between 1.4 m and 7.2 m; this results in different acceleration gradients along the body (in different centrifuges) for the same reference value at a given point on the body itself. Finally, the reference point along the *z*-axis for the acceleration measure was not uniform across studies: some of them report it at heart level (Konishi et al., 2019; Ogawa et al., 2016; Ueda et al., 2015) and others at foot level (Diaz-Artiles et al., 2018; Habazettl et al., 2016). Due to the aforementioned differences, the experimental data exploited to validate our model are inherently heterogeneous.

The model was validated against the experimental behaviour of six haemodynamic variables – which are the most commonly reported variables in the literature – in the gravity range from 0*g* to 2.5*g*. The variables considered are: heart rate (HR (bpm)), cardiac output (CO (l/min)), stroke volume (SV (ml)) mean arterial pressure (MAP (mmHg)), systolic arterial pressure (SAP (mmHg)), and diastolic arterial pressure (DAP (mmHg)). It is worth noting that both in centrifuge and parabolic flight studies, all authors measured the arterial blood pressure at the level of the finger. These measurements were corrected either by maintaining the hand at the same level of the heart or applying an appropriate pressure correction that accounts for the contribution of the hydrostatic term. In addition, some of these authors computed MAP, SAP and DAP after reconstructing the brachial artery pressure via a suitable transfer function. Conversely, in our model, MAP, SAP and DAP are computed at the level of the ascending aorta.

For each group of the dataset (centrifuges, parabolic flights at seated and standing posture), all haemodynamic variables were normalized with respect to the corresponding 1*g* values (the normogravity 1*g* condition is denoted as g_0). This normalization eliminates the heterogeneity in baseline mean values at 1*g* across individual studies, ensuring a direct focus on how

each cardiac parameter changes with g. Following normalization, the experimental data of each variable collected from the literature were pooled. In particular, the data pooling was carried out across each investigated gravity level. For instance, considering that centrifuge studies provided HR measurements at $g/g_0 = [0, 0.5, 1, 1.4, 1.5, 2, 2.5]$, the pooled mean ($\mu^{\mathrm{P}}$) and the pooled standard deviation (σ^{P}) were computed for each of these g values. It is important to note that the number of observations for each sample varies across the different studies. Therefore, values of μ^{P} and σ^{P} for each cardiac parameter X and gravity level j were computed as (Borenstein et al., 2009):

$$\mu^{\mathrm{P}}_{Xj} = \frac{\sum_{i=1}^{k} n_i \mu_{Xi,j}}{\sum_{i=1}^{k} n_i}, \tag{11}$$

$$\sigma^{\mathrm{P}}_{Xj} = \sqrt{\frac{\sum_{i=1}^{k} \sigma^2_{Xi,j}\,(n_i - 1) + \sum_{i=1}^{k} n_i \left(\mu_{Xi,j} - \mu^{\mathrm{P}}_{Xj}\right)^2}{\sum_{i=1}^{k} n_i - 1}}, \tag{12}$$

where n_i, $\mu_{Xi,j}$, $\sigma_{Xi,j}$ denote the number of samples, the mean, and standard deviation for the *X-th* cardiac parameter, at gravity level j, in the literature study i, respectively. Additionally, it should be mentioned that due to differences in experimental protocols, methods, and purposes among the extracted literature studies, not all provided experimental measurements for every cardiac parameter at each gravity level investigated. This heterogeneity resulted in a fragmented dataset, which did not allow for the computation of $\mu^{\mathrm{P}}{}_{Xj}$ and $\sigma^{\mathrm{P}}{}_{Xj}$ for certain cardiac parameters at specific g values. In particular, experimental measurements for SV and CO are missing at 2.5g, while data for SAP and DAP are not given at 0.5g. After determining the values of $\mu^{\mathrm{P}}{}_{Xj}$ and $\sigma^{\mathrm{P}}{}_{Xj}$ for each cardiac variable, a linear regression using the weighted least-squares fitting method was performed to verify the existence of a statistically significant trend with g. This approach enabled us to consider the impact of the different $\sigma^{\mathrm{P}}{}_{Xj}$ across the data by applying the weights $w_j = 1/(\sigma^{\mathrm{P}}{}_{Xj})^2$ in the formula for the sum of squared errors (Neter et al., 1996). Statistical significance of each trend was determined using a two-sided t test for the slope coefficient, with a significance level of 0.05.

Figure 2 shows, for each parameter, the model outcomes and the regression lines (dashed curves) alongside the pooled means $\mu^{\mathrm{P}}{}_{Xj}$ and the pooled standard deviation values $\sigma^{\mathrm{P}}{}_{Xj}$ (horizontal lines) of each dataset group collected from the literature.

Experimental data reveal an increasing trend in HR, MAP, SAP, and DAP, while SV and CO exhibit a decreasing behaviour. In particular, the linear regression analysis confirms that the trends in HR, MAP, SAP, DAP, and SV are statistically significant (p-value < 0.05), whereas CO fails to pass the t test, reporting a p-value of 0.13. In detail, as gravity increases from 0g to 2g, centrifuge data (red lines) show a −37.8% decrease in $\mu^{\mathrm{P}}{}_{\mathrm{SV}}$. Similarly, parabolic flight measures indicate reductions of −39.5% and −29.8% in the range [0g–1.8g] in standing (blue lines) and sitting positions (yellow lines), respectively (Fig. 2*A*). This behaviour is attributed to the fact that an increase in g triggers a fluid shift from the upper to lower regions of the body, leading to decreased venous return and reduced SV. To counteract this drop, short-term regulation mechanisms (arterial baroreflex and cardiopulmonary reflex) induce a rise in $\mu^{\mathrm{P}}{}_{\mathrm{HR}}$ (Fig. 2*B*): +57% from 0g to 2.5g, +33% and +12.8% from 0g to 1.8g in parabolic flights with standing and seated posture, respectively. As a result, CO remains relatively stable within the investigated range of gravity, explaining the non-significant trend in CO (Fig. 2*C*).

Observing the pressure data, systemic MAP (Fig. 2*D*) appears to increase with increasing gravitational force – $\mu^{\mathrm{P}}{}_{\mathrm{MAP}}$ rises by 11.2%, 16.2% and 16.8% for centrifuges, parabolic flight in standing and seated posture, respectively – mostly due to increased $\mu^{\mathrm{P}}{}_{\mathrm{DAP}}$ (Fig. 2*E*). With regard to SAP, the experimental data show some discrepancies. Specifically, $\mu^{\mathrm{P}}{}_{\mathrm{SAP}}$ (Fig. 2*F*) does not exhibit a clear trend in relation to gravity in centrifuge measures (red lines). Conversely, during parabolic flights, an increase of +19% is observed from 0g to 1.8g in the sitting position (yellow lines), whereas in the standing posture (blue lines), the initial elevation occurring from 0g to 1g is followed by a slight decline in the hyper-gravity range.

Our cardiovascular model gives values which generally align with the experimental data, and all model outcomes (reported in Fig. 2 through continuous black curves) fall within the range $\mu^{\mathrm{P}} \pm \sigma^{\mathrm{P}}$, indicating that the model is able to capture the cardiovascular response to gravity changes in both micro- and hyper-gravity conditions. In particular, SV (Fig. 2*A*) decreases by −46.1% within the range [0g–2g], in agreement with experimental data, and drops by −60.8% up to 3g, varying from 82.9 ml at 0g to 32.5 ml at 3g. Conversely, HR (Fig. 2*B*) initially exhibits a non-linear increase from 0g to 0.5g, followed by a linear behaviour beyond this value. Specifically, as gravitational acceleration varies from 0g to 3g, the model detects an increment of 94%, with HR growing from 66 bpm to 128 bpm. Moreover, a good correspondence between the predicted values for both SV and HR and their respective regression lines is observed. With regard to CO (Fig. 2*C*), the model predicts a slight monotonic decrease from 5.45 l/min at 0g to 4.16 l/min at 3g (−23.7%). Notably, although the weighted least-squares fitting analysis highlighted a weakly non-significant trend for CO, the slope of the data-based regression line is negative and closely aligns with the results provided by the model.

Due to the peripheral vascular adjustments governed by short-term regulation mechanisms, MAP (Fig. 2*D*) mildly increases from 92 mmHg at 0*g* to 96.2 mmHg at 1*g* (+4.6%). Beyond this value, MAP remains constant up to 2.2*g*, before gradually decreasing and returning to 92 mmHg at 3*g*. The model correctly predicts the increase in diastolic pressure (Fig. 2*E*). In particular, DAP grows monotonically from 0*g* to 2.5*g*, varying from 69 mmHg to 82 mmHg (+19%), while it remains quite constant from 2.5*g* to 3*g*. Concerning SAP (Fig. 2*F*), the model predicts a non-monotonic behaviour with *g*. The systolic pressure is constant at around 121 mmHg in the gravity range [0*g*–0.5*g*]. Beyond this range, SAP exhibits a monotonic decrease, reaching a value of 104 mmHg at 3*g*. This behaviour doesn't fully match with the fitting analysis, where a positive slope was found for SAP. However,

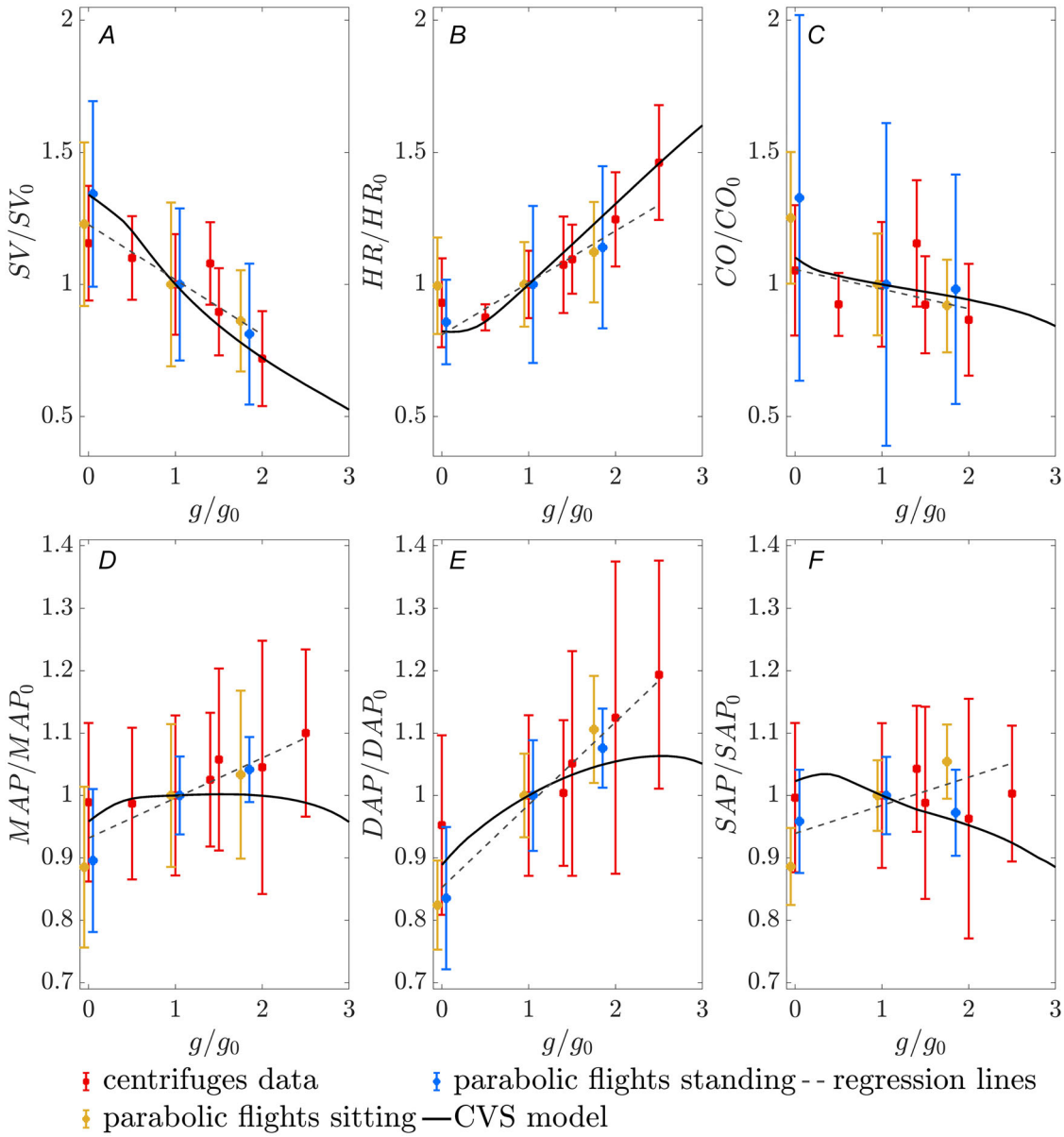

Figure 2. Pooled mean μ^{P}_{Xj} and standard deviation σ^{P}_{Xj}, for the *X-th* cardiac parameter at gravity level *j*
Data are reported as vertical red (centrifuges data), blue (parabolic flights data in standing posture), and yellow (parabolic flights data in sitting posture) points and lines. The model outcomes are depicted as black continuous curves, whereas the dashed curves represent the regression lines computed using the weighted least-squares fitting method. Trends in SV (*A*; *p*-value < 0.001), HR (*B*; *p*-value < 0.001), MAP (*D*; *p*-value < 0.001), SAP (*F*; *p*-value = 0.0161) and DAP (*E*; *p*-value < 0.001) are statistically significant, whereas CO (*C*) fails to pass the *t* test with a *p*-value equal to 0.130.

as above-mentioned, the experimental data are quite contradictory, and a decline in SAP is also observed during the hyper-gravity phase of parabolic flight in a standing posture (blue symbols). We recall that this posture, among all the experimental setups examined, is the most representative of that simulated by our model, which reproduces a uniform gravitational acceleration along the head-feet axis during exposure to gravity transitions in standing posture.

Results

The previous section allowed us to validate and compare our cardiovascular model with existing experimental data for the main central haemodynamic variables. Here, using our mathematical model, we will explore the response of cardiac parameters which are difficult to investigate experimentally, aiming to shed light on the cardiac function under altered gravitational force. In particular, the short-term cardiac response to gravity changes will be first investigated by means of the main mechano-energetic cardiac parameters and oxygen consumption indexes. Secondly, the perfusion of the myocardial tissue will be examined by focusing on both the left and right coronary circulations. Finally, the gravity impact on mean and pulsatile values of the central venous pressure (CVP), the pulmonary artery pressure (P_{pa}), the pulmonary capillary wedge pressure (PCWP), and the central aortic pressure (P_{aa}) will be evaluated.

Figure 3 illustrates the acute haemodynamic response of the left and right ventricles from micro- (0*g*) to hyper-gravity (3*g*). In particular, the response is investigated in terms of the cardiac parameters introduced in the section on Cardiac and coronary hemodynamic parameters.

The right and left ventricles PV loops (Fig. 3*A* and *B*) exhibit significantly different responses to gravity changes. As *g* varies from 0*g* to 3*g*, due to the reduced venous return at higher *g* values, both left and right end-diastolic volumes ($EDV_{lv/rv}$) decrease similarly between the two ventricles, with EDV_{lv} and EDV_{rv} varying from 133.0 to 67.7 ml and from 143.0 to 65.6 ml, respectively. A reduction in left and right end-systolic volumes ($ESV_{lv/rv}$) is also observed as *g* rises: ESV_{lv} decreases from 50.1 ml at 0*g* to 35.2 ml at 3*g*, whereas ESV_{rv} diminishes from 60.7 ml to 33.8 ml. Additionally, due to the reduced ventricular filling both left and right ventricular end-diastolic pressures ($EDP_{lv/rv}$) decrease monotonically with increasing *g*. However, this similar behaviour between the ventricles does not apply to end-systolic pressures ($ESP_{lv/rv}$). In the systemic circulation, the baroreceptors and cardiopulmonary reflexes induce an increase in total peripheral resistance, maintaining an adequate ESP_{lv} even at higher *g* values, with ESP_{lv} slightly decreasing from 96.6 mmHg at 0*g* to 86.6 mmHg at 3*g*. On the contrary, in the right ventricle, ESP_{rv} decreases from 15.1 mmHg at 0*g* to 2.23 mmHg at 3*g* (−85%). This entails a different behaviour of EW/min between the left and right ventricles (Fig. 3*C* and *D*). In particular, the decrease in EDV, elicited by the blood shift towards the lower extremities and the reduced venous return, affects the preload, reducing both the stroke volume and the EW via the Frank-Starling mechanism (Westerhof et al., 2019). However, while for the left ventricle, the PV loop shrinks primarily in a horizontal direction, thus limiting the reduction in EW/min, this does not occur for its right counterpart, where both a horizontal and vertical shortening of the PV loop is detected. Hence, the reduction in EW/min for the left ventricle is restricted to −15% up to 2.2*g* (from 76 J/min at 0*g* to 65 J/min at 2.2*g*). Beyond this value, EW/min decreases with a higher rate and a drop of −27% is detected at 3*g* with respect to 0*g*. Conversely, the rate of decrease in EW/min is almost constant for the right ventricle, and a reduction of −47% is observed as gravity rises from 0*g* to 3*g* (from 11.8 J/min to 6.2 J/min).

Differences between the right heart and the left heart are also noticeable in PE/min. In the left ventricle, the mechanical potential energy expressed per minute (Fig. 3*C*) does not exhibit large variations. In particular, it displays a non-monotonic trend, gradually increasing with gravitational acceleration and reaching a maximum at around 2.3*g* (from 21.5 J/min at 0*g* to 27.6 J/min at 2.3*g*, +28.4%). Beyond this peak, PE/min declines slightly, but remains higher compared to the value observed at 0*g*. In contrast, in the right ventricle, PE/min decreases monotonically from 4.4 J/min at 0*g* to 2.4 J/min at 3g (−45.5%), due to the abovementioned decline in ESP_{rv}.

Pressure-volume area PVA/min, which is given by the sum of PE/min and EW/min (see shaded areas in Fig. 3*A* and *B*), follows a similar response to that of EW/min in both ventricles. The strong dependence of PVA/min on EW/min is primarily due to the minor variations in PE/min with respect to the changes in EW/min as gravity rises. However, by observing the efficiency indexes LVE and RVE (Fig. 3*E* and *F*) – which are defined as the ratio EW/PVA – two different responses to gravity changes between left and right ventricles emerge due to the different behaviour of PE/min. In the left heart chamber, LVE decreases monotonically from 0.78 at 0*g* to 0.68 at 3*g* (−12.8%), whereas RVE is almost constant, varying from 0.73 to 0.72 (−1.4% from 0*g* to 3*g*).

In Fig. 3*E* and *F*, another index of cardiac efficiency, EF, is reported. EF expresses the emptying capability of the left/right ventricle during systole. This capability worsens similarly for both ventricles as gravity rises. The primary reason behind this decline is the reduction in SV (see Fig. 2*A*), which is equal for right and left ventricles. In particular, as gravity rises from 0*g* to 3*g*, EF decreases from

62% to 48% in the left ventricle and from 58% to 48% in the right one.

Finally, Fig. 3*G* illustrates the behaviours of the oxygen consumption indexes RPP and TTI/min. Both indexes exhibit a non-linear increase with *g*. TTI/min is characterized by a minimum in the proximity of 0.4*g*, followed by a central section where TTI/min increases, reaching a maximum close to 2.7*g*. However, as already observed in a previous study on the cardiovascular response to parabolic flights (Fois, Ridolfi, et al., 2022), TTI/min remains slightly affected by gravitational acceleration, with variations across the gravity range limited to −0.6% (at 0.4*g*) and to +7.7% (at 2.7*g*) with respect to the 0*g* condition. Conversely, RPP shows a +68.5% increase within the range [0*g*–3*g*]. Hence, the behaviours of both TTI/min and, especially, RPP suggest

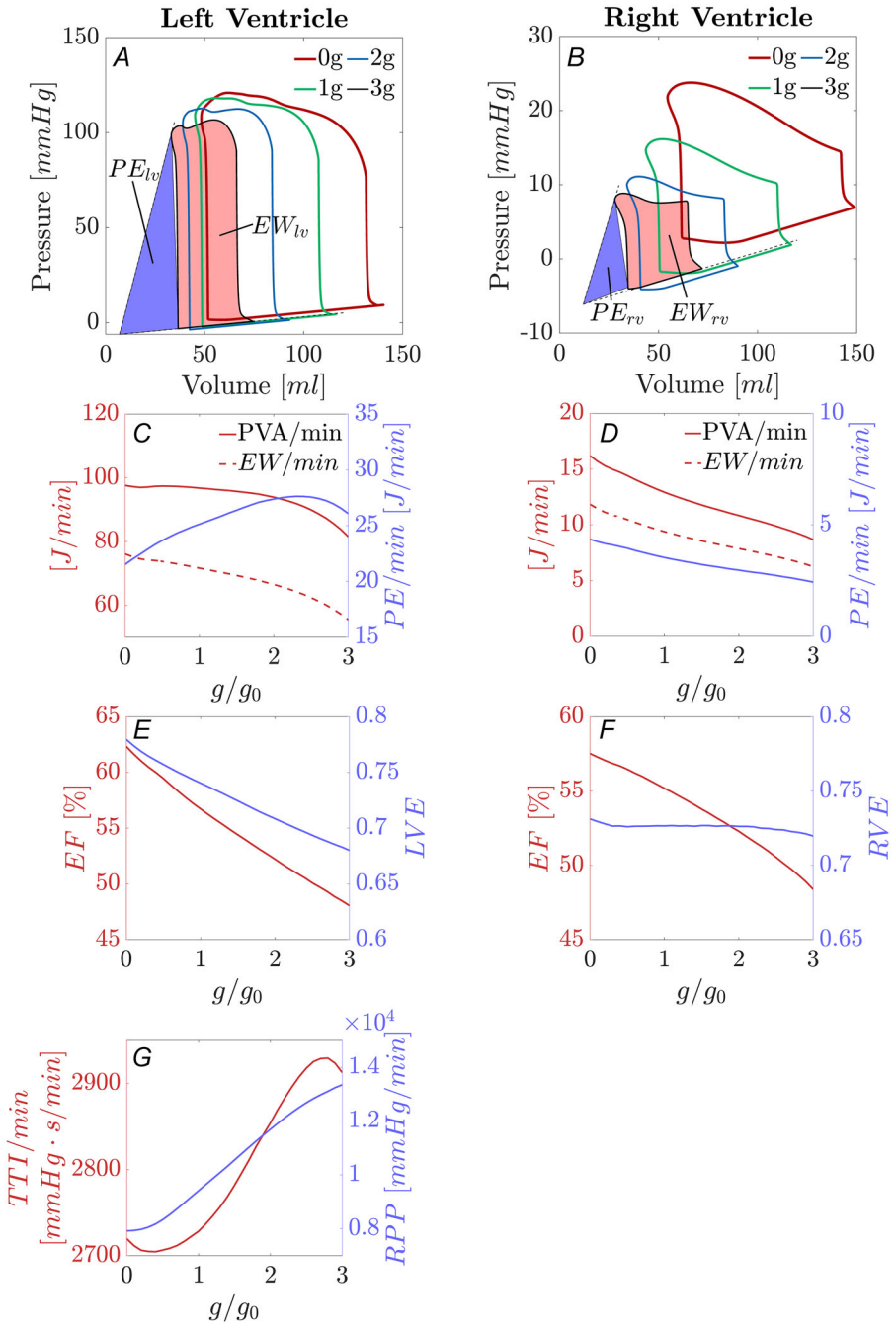

Figure 3. Response of left and right ventricles to gravity changes
Left and right columns report *PV* loops (*A* and *B*), mechano-energetics (*C* and *D*), efficiency (*E* and *F*) and oxygen consumption parameters (*G*) for left and right ventricles, respectively.

an increase in oxygen consumption and, therefore, in energy demand of the left ventricle at higher g values. Moreover, with EW/min being an index of the energy supply, comparison of EW/min and oxygen consumption indexes highlights a mismatch between the left ventricle energy supply and energy demand for increasing gravity levels.

In Fig. 4, the comparison between the short-term haemodynamic response of the left and right coronary circulations is reported. Coronary perfusion is evaluated at varying levels of gravitational acceleration in terms of coronary $SV_{LAD/RCA}$, $CBF_{LAD/RCA}$ and $CPP_{LAD/RCA}$ (see section on Cardiac and coronary hemodynamic parameters). Additionally, the LAD flow rate (Q_{LAD}) waveforms at four different levels of g are reported.

Figure 4*A* displays SV_{LAD}, SV_{RCA} and their SV_{LAD}/SV_{RCA} ratio. SV varies similarly with gravity in both LAD and RCA. Thus, the SV_{LAD}/SV_{RCA} ratio is barely affected by gravity changes, varying from 1.54 at 0g to 1.42 at 3g (−7.8%). Specifically, at low g values, a slight increment in SV is observed, which reaches a maximum in the proximity of 0.5g. Beyond this value, SV sharply decreases, falling by −26.8% and −32.4% from 0g to 3g in the RCA and LAD, respectively. This drop is primarily due to the increase in HR with g. In fact, as HR increases, the duration of the cardiac cycle (RR) reduces, leading to altered diastolic and systolic lengths (RR_{dia} and RR_{sys}). It follows that, as blood flow within the coronary arteries occurs mainly during diastole due to the mechanical compression exerted by the cardiac muscle in the systolic phase, the coronary perfusion changes. In particular, diastolic length suffers a more significant contraction compared to systole (RR_{dia} is 59.8% of RR at 0g and 43.3% of RR at 3g), resulting in a decreased RR_{dia}/RR_{sys} ratio and a reduced SV. This response is well captured in Fig. 4*B* and *C*, where the fractions of SV during diastolic and systolic phases (SV_{dia} and SV_{sys}) in LAD and RCA are reported at different levels of g: while SV_{sys} is almost constant throughout the gravity range both in LAD and RCA, SV_{dia} mirrors the same behaviour of total SV. Hence, the SV_{dia}/SV_{sys} ratio decreases with g, varying from 3.7 at 0g to 1.7 at 3g in the LAD, and from 1.5 and 1.1 in the RCA.

Despite an overall decrease in SV being observed as g rises, CBF (Fig. 4*D*) grows with g in both coronary arteries due to the rise in HR. However, CBF exhibits a non-linear trend characterized by a downward concavity which reduces its increase at higher g values: in the LAD, an increase of +31.7% is detected at 3g with respect to 0g, whereas CBF rises by 42.5% in the RCA. Additionally, recalling that an increase in RPP of +68.5% is detected at 3g (recall Fig. 3*D*), the non-linear behaviour of CBF suggests an imbalance of the energy supply/demand ratio even at coronary level during hyper-gravity exposure.

CPP (in Fig. 4*E*) displays a similar behaviour to that of CBF in both coronary arteries. We recall that CPP is often used as a surrogate for CBF (Koeppen & Stanton, 2023). According to its formulation, CPP is strictly associated with aortic diastolic pressure. Therefore, the increment in DAP with g is the main cause of CPP behaviour. Moreover, the CPP_{LAD}/CPP_{RCA} ratio is constant throughout the gravity range and is equal to 0.93 (not shown in Fig. 4*E*), thus highlighting no impairment between right and left CPP as g varies.

Figure 4*F* highlights the impact of g on Q_{LAD} by showing the flow rate waveforms at four different levels of g (0g, 1g, 2g and 3g). As g increases from 0g to 3g, the waveform undergoes significant changes mainly during diastole. In fact, besides a temporal shortening due to the rise in HR, an amplitude stretch is observed, with the diastolic peak growing with rising g. At lower g values, the diastolic maximum peak is followed by a slow decreasing phase. This feature is completely lost at higher g due to the contraction of the diastole duration. Consequently, the systole begins with significantly higher Q_{LAD} values. This is the most significant change that can be detected during the systolic phase. Additionally, Fig. 4*G* and *H* illustrates how the length of the cardiac cycle affects the SV_{dia}/SV_{sys} ratio as g varies from 0g to 3g. The impact of HR on the imbalance of the RR_{dia}/RR_{sys} ratio is clearly observed, with the ratio decreasing from 1.49 at 0g to 0.76 at 3g. Hence, at 3g the systolic phase becomes predominant over diastole, resulting in the aforementioned drop of the SV_{dia}/SV_{sys} ratio.

In Fig. 5, the mean values and amplitudes (computed as the difference between maximum and minimum values) of the central aortic pressure (P_{aa}), central venous pressure (CVP), pulmonary artery pressure (P_{pa}), and pulmonary capillary wedge pressure (PCWP) are displayed as function of the gravitational acceleration. These pressures provide crucial information regarding the overall haemodynamic status of the heart. In fact, P_{aa} and P_{pa} represent the pressure level at the left and right ventricular outlets, whereas CVP and PCWP reflect the pressure within the right and left atria, respectively.

Figure 5*A* shows how mean and pulsatile values within the aortic root ($\overline{P_{aa}}$ and ΔP_{aa}, respectively) vary with g. Specifically, $\overline{P_{aa}}$ initially increases with g, varying from 92 mmHg at 0g to 96.2 mmHg at 1g. This slight increase is due to the inotropic effect and the heightened peripheral vascular resistance triggered by short-term regulation mechanisms. $\overline{P_{aa}}$ is nearly constant up to 2g, maintaining a value close to 96 mmHg, whereas at 3g a moderate decrease is detected, with $\overline{P_{aa}}$ reaching 92 mmHg. Due to the almost opposite behaviour of DAP and SAP, ΔP_{aa} decreases with rising g, reducing from 51.7 mmHg at 0g to 23.0 mmHg at 3g (−55.5%). This decline in ΔP_{aa} reflects the drop in the left ventricle SV, confirming

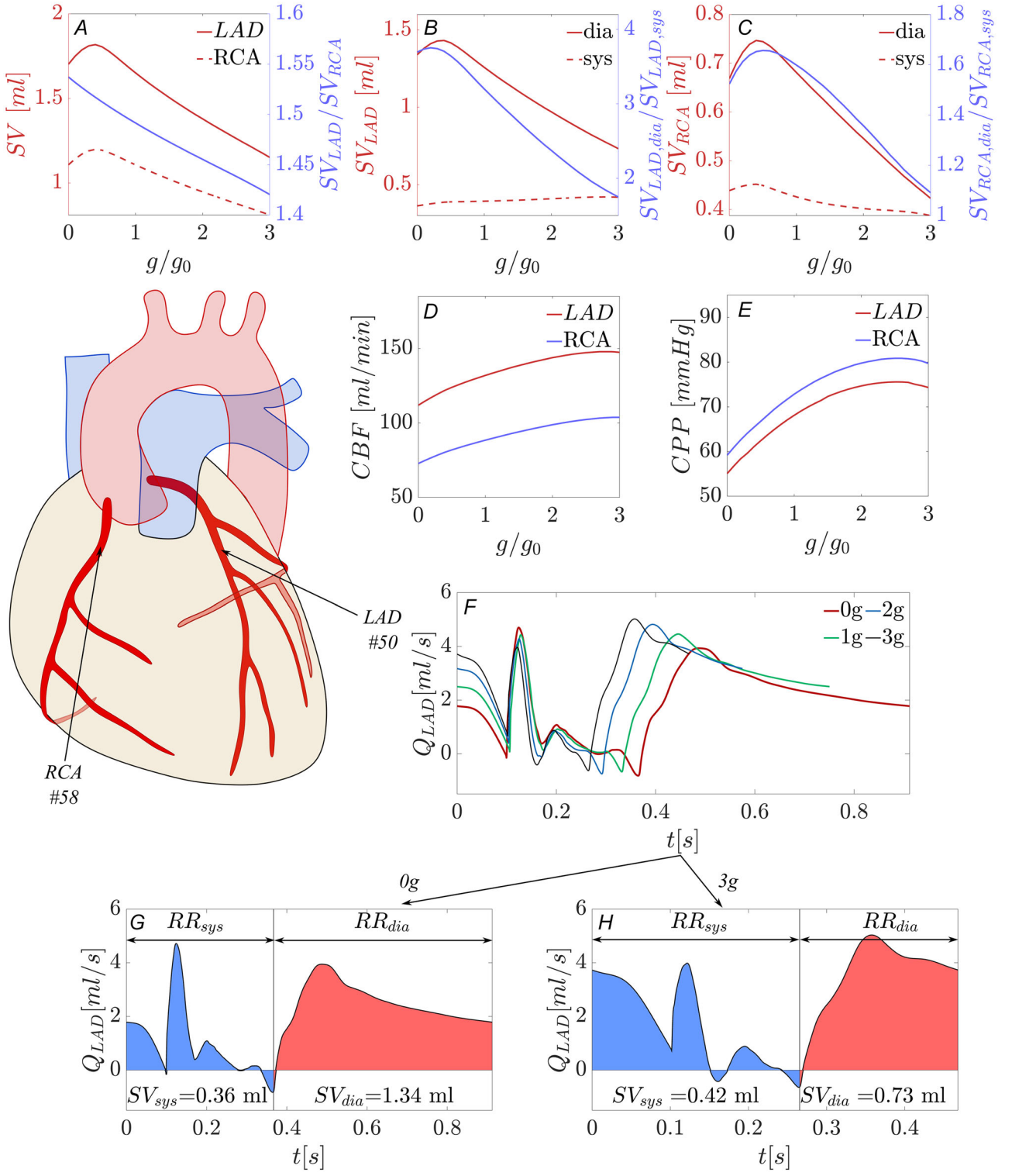

Figure 4. Response of coronary circulation to gravity changes
Coronary blood flow and coronary perfusion parameters: *A* shows the coronary stroke volume in the LAD (SV_{LAD}) and RCA (SV_{RCA}) along with the SV_{LAD}/SV_{RCA} ratio; *B* and *C* show the SV partition between diastolic and systolic phases; *D* and *E* illustrate the coronary blood flow (CBF) and the coronary perfusion pressure (CPP), respectively; *F–H* show the impact of gravity changes on Q_{LAD} waveform.

the close relationship between these two haemodynamic parameters (Hall & Hall, 2020).

CVP, mean pulmonary arterial pressure ($\overline{P_{pa}}$) and PCWP (Fig. 5*B*–*D*) are significantly affected by gravity acceleration and, contrary to $\overline{P_{aa}}$, exhibit a (non-linear) decreasing trend with increasing g. These pressures are characterized by much lower values than central aortic pressure and, therefore, are more susceptible to changes in intrathoracic pressure (ITP). Specifically, at higher g values the diaphragm is pulled towards the abdominal cavity, leading to a reduction in ITP (Peterson et al., 2002; Videbaek & Norsk, 1997). Hence, the mean values of CVP and PCWP follow a similar decreasing behaviour, reducing from 6.6 mmHg to −1 mmHg (−115% from 0g to 3g) and from 8.1 mmHg to 0.5 mmHg (−94% from 0g to 3g), respectively. With regard to pulsatile values of the pressure within the right and left atria, both decrease with rising g, as a result of the progressively reduced venous return and the subsequent decrease in atrial filling elicited by the increasing gravitational force. Similarly, both the mean and pulsatile values of P_{pa} exhibit a monotonic decline, diminishing from 15.4 mmHg to 5.5 mmHg (−64.3% from 0g to 3g) and from 13.9 mmHg to 6.3 mmHg (−54.7% from 0g to 3g), respectively. Notably, the trends observed for $\overline{P_{pa}}$, $\overline{CVP}$ and $\overline{PWCP}$ decrease non-linearly with g. In particular, most of the drop occurs within the gravity range [0g–2g], with minor variations in the upper region of the investigated hyper-gravity range.

Discussion

The existing literature on cardiac function under altered gravity conditions appears rather fragmented and characterized by several sources of uncertainty. The limited number of studies, the challenges in acquiring clinical measures in difficult conditions, and the significant inter- and intra-study differences restrict our knowledge of the cardiovascular response to a small set of haemodynamic parameters (Blaber et al., 2010; Goswami et al., 2021; Hughson et al., 2018; Norsk, 2020; Shen & Frishman, 2019; Zhu et al., 2015). As a result, information is lacking regarding several key aspects of cardiac behaviour, such as energy performance, oxygen consumption, right heart function, and coronary perfusion at different levels of gravitational force. In order

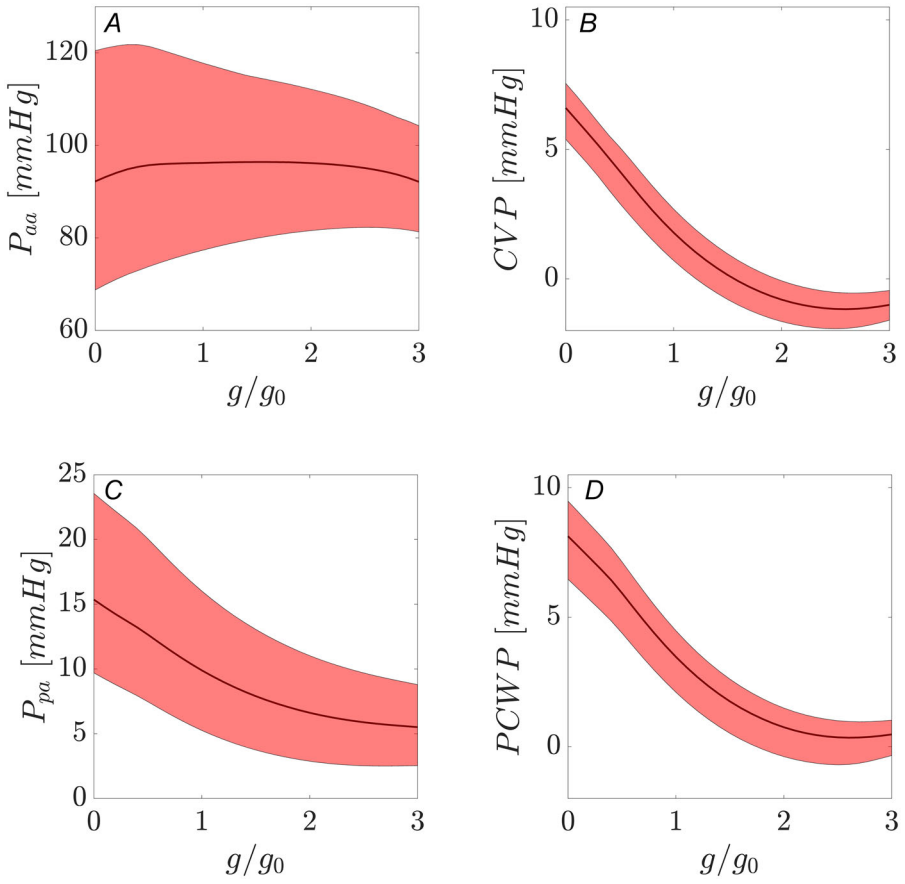

Figure 5. Response of cardiac inlet and outlet pressures to gravity changes
Mean values (continuous lines) and amplitudes (shaded area) of: *A*, ascending aortic pressure; *B*, central venous pressure; *C*, pulmonary artery pressure; and *D*, pulmonary capillary wedge pressure.

Table 1. Key findings of the cardiac function in micro- ([0*g*–1*g*]) and hyper-gravity ([1*g*–3*g*])

Haemodynamic parameters		[0*g*–1*g*]		[1*g*–3*g*]	
Left heart	Mechano-energetic	PV loop	Shifts and stretches horizontally	PV loop	Shifts and shrinks horizontally
		EW/min	≈↑ (+6%)	EW/min	↓ (−22.6%)
		PVA/min	≈ (+0.8%)	PVA/min	↓ (−15.7%)
	Oxygen consumption	RPP	↓ (−15.9%)	RPP	↑↑ (+41.8%)
		TTI/min	≈ (−0.3%)	TTI/min	≈↑ (+6.8%)
	Efficiency	EF	↑ (+9.9%)	EF	↓ (−15.3%)
		LVE	≈↑ (+5.3%)	LVE	≈↓ (−8.1%)
Right heart	Mechano-energetic	PV loop	Shifts and stretches vertically and horizontally	PV loop	Shifts and shrinks vertically and horizontally
		EW/min	↑ (+26.0%)	EW/min	↓↓ (−33.5%)
		PVA/min	↑ (+25.5%)	PVA/min	↓↓ (−32.9%)
	Efficiency	EF	≈↑ (+4.2%)	EF	↓ (−12.3%)
		RVE	≈ (+0.6%)	RVE	≈ (−0.9%)
Coronary perfusion		SV	↑	SV	↓
		CBF	↓	CBF	↑
		CPP	↓	CPP	↑
		Amplitude and shape changes of Q_{LAD} signals as *g* increases from 0g to 3g			
Central pressures	Mean values	P_{aa}	≈	P_{aa}	≈
		P_{pa}	↑	P_{pa}	↓
		CVP	↑	CVP	↓
		PCWP	↑	PCWP	↓
	Amplitude	P_{aa}	↑	P_{aa}	↓↓
		P_{pa}	↑	P_{pa}	↓↓
		CVP	≈↑	CVP	↓↓
		PCWP	↑	PCWP	↓↓

≈, no clear trend; ≈↑ or ≈↓, slight increase or decrease; ↑ or ↓, increase or decrease; ↑↑ or ↓↓, great increase or decrease.

to shed light on these gaps, in this work, we have exploited our mathematical framework to provide novel insights into left and right cardiac haemodynamics within the gravity range [0*g*–3*g*].

The results, as summarized in Table 1, indicate that transitions from micro- to hyper-gravity elicit different left and right heart haemodynamics responses. Within the hypo-gravity range (i.e. [0*g*–1*g*]), the venous return is increased due to fluid shift from the caudal to the cranial region. Consequently, in micro-gravity, both the left and right ventricular chambers receive a larger quantity of blood, with both end-systolic and end-diastolic volumes increasing as gravity approaches 0*g*, resulting in an increased ventricular preload. However, as depicted in Fig. 3, the left ventricular PV loop exhibits a horizontal shift, whereas in the right ventricle, both horizontal and vertical shifts are detected, as both end-systolic and end-diastolic pressures increase when entering the hypo-gravity range. This different behaviour between left and right ventricles was already observed by Gerber et al. (2018), who suggested that an increase in CVP is responsible for this right ventricular PV loop upward shift. In agreement with this observation, our cardiovascular model predicts an increase in CVP (from 1.8 mmHg at 1*g* to 6.6 mmHg at 0*g*) during short-term micro-gravity exposure in standing posture. However, actual spaceflight data on CVP reveal some discrepancies. For instance, Buckey et al. (1996) reported a decrease in CVP during micro-gravity with respect to supine and seated pre-flight values, whereas Foldager et al. (1996) detected an increase in CVP both in seated and standing postures. In addition to the rise in CVP, the upward shift of the right ventricular PV loop could be explained by reduced activity of short-term regulation mechanisms for the cardiopulmonary circulation, such as the baroreceptor and cardiopulmonary reflexes. In systemic circulation, these mechanisms regulate total peripheral resistance to maintain adequate arterial pressure across a wide range of gravitational acceleration (see Fig. 5*A*). In contrast, the total resistance of the pulmonary circulation is governed by other factors, such as respiratory gases, humoral and neural mechanisms (Barnes & Liu, 1995). Our mathematical model does not implement these mechanisms, resulting in a constant pulmonary vascular resistance throughout the entire gravity range. Consequently, the micro-gravity-induced

increase in stroke volume and cardiac output leads to elevated right ventricle end-systolic and diastolic pressures. As a result, the right ventricle PV loop is more affected by gravity variations than its left counterpart. This is also evident from the analysis of the mechano-energetic parameters. Specifically, as gravity varies from 1*g* to 0*g*, EW/min increases by +6% in the left ventricle (from 71.6 J/min at 1*g* to 76.1 J/min at 0*g*) and by +26% in the right ventricle (from 9.4 J/min at 1*g* to 11.8 J/min at 0*g*), respectively. Moreover, PVA/min, which represents the total mechanical energy produced by ventricular contraction, is almost constant for the left ventricle (+0.8% from 1*g* to 0*g*), whereas an increase of +25.5% is detected in PVA_{rv}/min. Additionally, together with a rise in the mechano-energetic indexes, a reduction in oxygen consumption parameters (i.e. RPP and TTI/min) and an increase in cardiac efficiency (i.e. $EF_{lv/rv}$, LVE and RVE) are observed, suggesting that cardiac performance is enhanced during short-term exposure to micro-gravity.

In the hyper-gravity range (i.e. [1*g*–3*g*]), a reduction in both PV loop widths is observed (see Fig. 3*A* and *B*), affecting both SV and left/right cardiac performance. Due to the above-mentioned different response between left and right ventricles, the right PV loop also shrinks in the vertical direction. However, in contrast to micro-gravity, short-term exposure to hyper-gravity elicits a significant decrease in both the left and right EW/min: EW_{lv}/min decreases by −22.6% and EW_{rv}/min diminishes by −33.5% as *g* rises from 1*g* to 3*g*. Since EW/min is a proxy of cardiac energy supply (Koeppen & Stanton, 2023; Westerhof et al., 2019), its decrease indicates a loss of cardiac performance, which no longer appears sufficient during hyper-gravity exposure. In this context, our model outputs show that an increase in *g* is associated with an increment in oxygen consumption indexes RPP and TTI/min. In particular, RPP increases by +41.8% as gravitational force varies from 1*g* to 3*g*. This indicates that the cardiac energy demand in hyper-gravity is notably increased. Consequently, taking into account the simultaneous drop in EW/min, our simulations suggest an imbalance between the energy demand and supply within the hyper-gravity range. Impairment of cardiac performance is further supported by the behaviour of the ventricular efficiency indexes: LVE, EF_{lv} and EF_{rv} decrease monotonically with increasing *g*, while RVE is nearly constant. Specifically, at 3*g*, both ejection fractions fall below 50%. This value is critical, with EF values between 40% and 49% being associated with heart failure with mildly reduced ejection fraction (Savarese et al., 2022).

The hyper-gravity scenario is further complicated by an impairment between myocardial oxygen demand and coronary perfusion. Specifically, the increase in HR, induced by the baroreflex, elicits an altered RR_{sys}/RR_{dia} ratio, increasing the systolic phase over the diastolic duration. This results in a $SV_{LAD/RCA}$ reduction, which is only partially mitigated by HR. In fact, both CBF_{LAD} and CBF_{RCA} increase non-linearly, exhibiting a downward concavity and reaching a maximum in the proximity of 2.8*g*. Hence, at higher *g* values the increase in CBF is slowed down, failing to compensate for the larger rise in RPP, thus producing an energy mismatch even at the coronary level. Similar findings have been observed in studies of coronary circulation during arrhythmias at varying heart rates (Gamilov et al., 2020; Scarsoglio et al., 2019). Additionally, our numerical model allowed us to analyse the flow rate waveform in the left ascending coronary artery, highlighting both amplitude and shape distortions of Q_{LAD} signals as *g* increases from 0*g* to 3*g*.

One of the advantages of our mathematical framework is that it allows for a direct investigation of mean and pulsatile values of the pressure signal in regions of the cardiovascular system that are challenging to access using current measurement methods. In this context, we evaluated the behaviour of mean and pulsatile values of the pressure at the initial and final sites of the systemic (P_{aa} and CVP) and cardiopulmonary (P_{pa} and PCWP) circulations, respectively. The cardiovascular model highlights a different behaviour between the mean values of P_{aa} and the mean values of CVP, P_{pa} and PCWP. The latter (CVP, P_{pa} and PCWP) are more susceptible to changes in intrathoracic pressure with respect to aortic pressure, which, instead, remains stable across the entire range of gravitational acceleration. Additionally, the absence of a regulation mechanism similar to that of the baroreceptors contributes to the decline in P_{pa} mean values as *g* increases. Consequently, the driving pressures of the systemic (P_{aa} − CVP) and cardiopulmonary (P_{pa} − PCWP) circulations respond differently: at 3*g* with respect to 0*g*, the driving pressure varies by +13% in the systemic circulation and by −30% in the cardiopulmonary circulation. Conversely, the pulsatility of these pressures exhibits similar behaviour with *g* variation. Specifically, an increment in all the pulsatilities is observed in the hypo-gravity range (from 1*g* to 0*g*: +28.0% for ΔP_{aa}, +28.8% for ΔP_{pa}, +8.7 for ΔCVP, and +26.8 for ΔPCWP), whereas the exact opposite is detected in the hyper-gravity range (from 1*g* to 3*g*: −43.2% for ΔP_{aa}, −41.9\% for ΔP_{pa}, −42.3 for ΔCVP, and −42.6 for ΔPCWP). This behaviour is due to the strong association between the stroke volume and pressure pulsatility (Hall & Hall, 2020).

The present mathematical framework has some limiting aspects. Specifically, each model parameter has a degree of uncertainty, which is challenging to quantify due to the high inter-subject variability. These parameters are influenced by several factors, including the subject's sex, anthropometric features and age. In this context, future studies could investigate how some parameters affect the cardiac response to gravity changes, addressing important physiological and medical issues such as

arterial ageing, individual variability for subject-specific applications, and gender differences. In addition, our model does not account for muscular activation – which may play an important role in venous return to the heart, especially during hyper-gravity exposure – and neglects the influence of tissue weight. The implemented regulation mechanisms are limited to the baroreceptor and the cardiopulmonary reflexes, thus neglecting other mechanisms, such as metabolic regulation and reactivity to CO_2 and O_2 concentrations. Furthermore, in our model, the pulmonary vascular resistance is assumed to be constant, whereas it is known to be non-linear and dependent on active (respiratory gases, humoral and neural mechanisms) and passive factors (cardiac output, left atrial pressure, airway and interstitial pressure) (Barnes & Liu, 1995). Finally, long-term regulation mechanisms related to renal, hormonal activity and trans-capillary blood flow are not described. A reduction (even partial) in these limitations will be needed for future studies aiming to investigate the long-term cardiovascular response.

Conclusions

The cardiovascular model described in this study provides valuable insights into cardiac function under micro- and hyper-gravity conditions, demonstrating a valid approach for investigating haemodynamic parameters which are challenging to measure directly using current acquisition methodologies. To the authors' knowledge, for the first time, the cardiac response across the entire spectrum from micro- to hyper-gravity is described in depth, and some crucial aspects emerge clearly. Firstly, the different behaviour between the left and right hearts, with the latter being more susceptible to gravity changes in terms of pressure and energy supply (EW/min). Secondly, our findings indicated that, in the short-term, micro-gravity exerts less stress on the heart due to enhanced venous return and ventricular filling, leading to improved cardiac energy performance and efficiency. Conversely, hyper-gravity imposes more stress on the cardiovascular system, leading to an energy supply/demand imbalance at both the cardiac and coronary levels. In particular, within the coronary circulation, the increase in HR at higher g values was insufficient to compensate for the reduction in coronary stroke volume, which occurred due to the reduced RR_{dia}/RR_{sys} ratio. Finally, our study highlighted that gravity significantly affects both mean and pulsatile values of central pressures, with increased pulsatility in micro-gravity and reduced pulsatility in hyper-gravity.

The picture of cardiac behaviour under gravitational stress outlined in this work opens the way to the study of the consequences that it has on other body regions. In this regard, it is sufficient to mention that higher pulsatility at the central level is typically associated with elevated variability in both cerebral blood flow and intracranial pressure (Scarsoglio et al., 2023). Since alterations in CBF and ICP, along with variations in intraocular pressure, are implicated in the onset of SANS, it follows that gravity-induced alteration of the cardiac response plays a crucial role in one of the most serious pathologies that can affect astronauts.

Our work demonstrates that mathematical modelling can usefully complement the usual clinical and experimental approaches, helping to shed light on currently unclear physiological and pathological mechanisms, with the aim of identifying effective countermeasures to be adopted in space flights.

References

Anselmino, M., Scarsoglio, S., Saglietto, A., Gaita, F., & Ridolfi, L. (2016). Transient cerebral hypoperfusion and hypertensive events during atrial fibrillation: A plausible mechanism for cognitive impairment. *Scientific Reports*, **6**(1), 28635.

Arbeille, P., Fomina, G., Roumy, J., Alferova, I., Tobal, N., & Herault, S. (2001). Adaptation of the left heart, cerebral and femoral arteries, and jugular and femoral veins during short- and long-term head-down tilt and spaceflights. *European Journal of Applied Physiology*, **86**(2), 157–168.

Barnes, P. J., & Liu, S. F. (1995). Regulation of pulmonary vascular tone. *Pharmacological Reviews*, **47**(1), 87–131.

Beckers, F., Seps, B., Ramaekers, D., Verheyden, B., & Aubert, A. E. (2003). Parasympathetic heart rate modulation during parabolic flights. *European Journal of Applied Physiology*, **90**(1–2), 83–91.

Berdahl, J. P., Yu, D. Y., & Morgan, W. H. (2012). The translaminar pressure gradient in sustained zero gravity, idiopathic intracranial hypertension, and glaucoma. *Medical Hypotheses*, **79**(6), 719–724.

Blaber, E., Marçal, H., & Burns, B. P. (2010). Bioastronautics: The influence of microgravity on astronaut health. *Astrobiology*, **10**(5), 463–473.

Blomqvist, C. G., & Stone, H. L. (1983). Cardiovascular adjustments to gravitational stress. *Comprehensive Physiology* (pp. 1025–1063).

Borenstein, M., Hedges, L. V., Higgins, J. P. T., & Rothstein, H. R. (2009). *Introduction to meta-analysis*. Wiley. https://onlinelibrary.wiley.com/doi/book/10.1002/9780470743386

Buckey, J. C. (2006). *Space physiology*. Oxford University Press.

Buckey, J. C., Gaffney, F. A., Lane, L. D., Levine, B. D., Watenpaugh, D. E., Wright, S. J., Yancy, C. W., Meyer, D. M., & Blomqvist, C. G. (1996). Central venous pressure in space. *Journal of Applied Physiology*, **81**(1), 19–25.

Burton, R. R. (1988). A human-use centrifuge for space stations: Proposed ground-based studies. *Aviation Space and Environmental Medicine*, **59**(6), 579–582.

Caiani, E. G., Sugeng, L., Weinert, L., Capderou, A., Lang, R. M., & Vaïda, P. (2006). Objective evaluation of changes in left ventricular and atrial volumes during parabolic flight using real-time three-dimensional echocardiography. *Journal of Applied Physiology*, **101**(2), 460–468.

Caiani, E. G., Weinert, L., Takeuchi, M., Veronesi, F., Sugeng, L., Corsi, C., Capderou, A., Cerutti, S., Vaïda, P., & Lang, R. M. (2007). Evaluation of alterations on mitral annulus velocities, strain, and strain rates due to abrupt changes in preload elicited by parabolic flight. *Journal of Applied Physiology*, **103**(1), 80–87.

Canuto, D., Chong, K., Bowles, C., Dutson, E. P., Eldredge, J. D., & Benharash, P. (2018). A regulated multiscale closed-loop cardiovascular model, with applications to hemorrhage and hypertension. *International Journal for Numerical Methods in Biomedical Engineering*, **34**(6), e2975.

Clément, G. (2011). *Fundamentals of space medicine*. Springer.

Clément, G. R., Bukley, A. P., & Paloski, W. H. (2015). Artificial gravity as a countermeasure for mitigating physiological deconditioning during long-duration space missions. *Frontiers in Systems Neuroscience*, **9**, 92.

Convertino, V. A. (1998). High sustained +gz acceleration: Physiological adaptation to high-G tolerance. *Journal of Gravitational Physiology*, **5**(1), P51–P54.

Diaz-Artiles, A., Heldt, T., & Young, L. R. (2018). Short-term cardiovascular response to Short-radius centrifugation with and without ergometer exercise. *Frontiers in Physiology*, **9**, 1492.

Diaz-Artiles, A., Heldt, T., & Young, L. R. (2019). Computational model of cardiovascular response to centrifugation and lower body cycling exercise. *Journal of Applied Physiology*, **127**(5), 1453–1468.

Fois, M., Diaz-Artiles, A., Zaman, S. Y., Ridolfi, L., & Scarsoglio, S. (2024). Linking cerebral hemodynamics and ocular microgravity-induced alterations through an in silico-in vivo head-down tilt framework. *Nature Partner Journals Microgravity*, **10**(1), 22.

Fois, M., Maule, S. V., Giudici, M., Valente, M., Ridolfi, L., & Scarsoglio, S. (2022). Cardiovascular response to posture changes: Multiscale modeling and in vivo validation during head-up tilt. *Frontiers in Physiology*, **13**, 826989.

Fois, M., Ridolfi, L., & Scarsoglio, S. (2022). In silico study of the posture-dependent cardiovascular performance during parabolic flights. *Acta Astronautica*, **200**, 435–447.

Foldager, N., Andersen, T. A., Jessen, F. B., Ellegaard, P., Stadeager, C., Videbaek, R., & Norsk, P. (1996). Central venous pressure in humans during microgravity. *Journal of Applied Physiology*, **81**(1), 408–412.

Fontolliet, T., Pichot, V., Antonutto, G., Bonjour, J., Capelli, C., Tam, E., Barthélémy, J.-C., & Ferretti, G. (2015). Effects of gravitational acceleration on cardiovascular autonomic control in resting humans. *European Journal of Applied Physiology*, **115**(7), 1417–1427.

Gallo, C., Ridolfi, L., & Scarsoglio, S. (2020). Cardiovascular deconditioning during long-term spaceflight through multiscale modeling. *Nature Partner Journals Microgravity*, **6**(1), 27.

Gamilov, T., Kopylov, P., Serova, M., Syunyaev, R., Pikunov, A., Belova, S., Liang, F., Alastruey, J., & Simakov, S. (2020). Computational analysis of coronary blood flow: The role of asynchronous pacing and arrhythmias. *Mathematics*, **8**(8), 1205.

Gerber, B., Singh, J.-L., Zhang, Y., & Liou, W. (2018). A computer simulation of short-term adaptations of cardiovascular hemodynamics in microgravity. *Computers in Biology and Medicine*, **102**, 86–94.

Goswami, N., Bruner, M., Xu, D., Bareille, M.-P., Beck, A., Hinghofer-Szalkay, H., & Blaber, A. P. (2015). Short-arm human centrifugation with 0.4g at eye and 0.75g at heart level provides similar cerebrovascular and cardiovascular responses to standing. *European Journal of Applied Physiology*, **115**(7), 1569–1575.

Goswami, N., White, O., Blaber, A., Evans, J., van Loon, J., & Clement, G. (2021). Human physiology adaptation to altered gravity environments. *Acta Astronautica*, **189**, 216–221.

Grigoriev, A. I., Kotovskaya, A. R., & Fomina, G. A. (2011). The human cardiovascular system during space flight. *Acta Astronautica*, **68**(9-10), 1495–1500.

Habazettl, H., Stahn, A., Nitsche, A., Nordine, M., Pries, A. R., Gunga, H.-C., & Opatz, O. (2016). Microvascular responses to (hyper-)gravitational stress by short-arm human centrifuge: Arteriolar vasoconstriction and venous pooling. *European Journal of Applied Physiology*, **116**(1), 57–65.

Hall, J. E., & Hall, M. E. (2020). *Guyton and Hall Textbook of Medical Physiology E-Book: Guyton and Hall Textbook of Medical Physiology E-Book*. Elsevier Health Sciences.

Hargens, A. R., Bhattacharya, R., & Schneider, S. M. (2013). Space physiology VI: Exercise, artificial gravity, and countermeasure development for prolonged space flight. *European Journal of Applied Physiology*, **113**(9), 2183–2192.

Hargens, A. R., & Richardson, S. (2009). Cardiovascular adaptations, fluid shifts, and countermeasures related to space flight. *Respiratory Physiology & Neurobiology*, **169**, S30–S33.

Heldt, T., Shim, E. B., Kamm, R. D., & Mark, R. G. (2002). Computational modeling of cardiovascular response to orthostatic stress. *Journal of Applied Physiology*, **92**(3), 1239–1254.

Holmlund, P., Eklund, A., Koskinen, L.-O. D., Johansson, E., Sundström, N., Malm, J., & Qvarlander, S. (2018). Venous collapse regulates intracranial pressure in upright body positions. *American Journal of Physiology-Regulatory, Integrative and Comparative Physiology*, **314**(3), R377–R385.

Hughson, R. L., Helm, A., & Durante, M. (2018). Heart in space: Effect of the extraterrestrial environment on the cardiovascular system. *Nature Reviews Cardiology*, **15**(3), 167–180.

Karmali, F., & Shelhamer, M. (2008). The dynamics of parabolic flight: Flight characteristics and passenger percepts. *Acta Astronautica*, **63**(5–6), 594–602.

Klein, T., Wollseiffen, P., Sanders, M., Claassen, J., Carnahan, H., Abeln, V., Vogt, T., Strüder, H. K., & Schneider, S. (2019). The influence of microgravity on cerebral blood flow and electrocortical activity. *Experimental Brain Research*, **237**(4), 1057–1062.

Koeppen, B. M., & Stanton, B. A. (2023). *Berne and Levy Physiology E-Book: Berne and Levy Physiology E-Book* (8th edn, Hall JM & Swiatecka-Urban A, Eds.). Elsevier Health Sciences. https://shop.elsevier.com/books/berne-and-levy-physiology/hall/978-0–323-84790-2

Konishi, T., Kurazumi, T., Kato, T., Takko, C., Ogawa, Y., & Iwasaki, K. (2019). Changes in cerebral oxygen saturation and cerebral blood flow velocity under mild +gz hypergravity. *Journal of Applied Physiology*, **127**(1), 190–197.

Lalande, S., & Buick, F. (2009). Physiologic +gz tolerance responses over successive +gz exposures in simulated air combat maneuvers. *Aviation Space and Environmental Medicine*, **80**(12), 1032–1038.

Lathers, C. M., Charles, J. B., Elton, K. F., Holt, T. A., Mukai, C., Bennett, B. S., & Bungo, M. W. (1989). Acute hemodynamic responses to weightlessness in humans. *The Journal of Clinical Pharmacology*, **29**(7), 615–627.

Liu, J., Verheyden, B., Beckers, F., & Aubert, A. E. (2012). Haemodynamic adaptation during sudden gravity transitions. *European Journal of Applied Physiology*, **112**(1), 79–89.

Lu, K., Clark, J. W., Ghorbel, F. H., Ware, D. L., & Bidani, A. (2001). A human cardiopulmonary system model applied to the analysis of the Valsalva maneuver. *American Journal of Physiology-Heart and Circulatory Physiology*, **281**(6), H2661–H2679.

Mukai, C. N., Lathers, C. M., Charles, J. B., Bennett, B. S., Igarashi, M., & Patel, S. (1991). Acute hemodynamic responses to weightlessness during parabolic flight. *The Journal of Clinical Pharmacology*, **31**(10), 993–1000.

Neter, J., Kutner, M. H., Nachtsheim, C. J., Wasserman, W., & others (1996). *Applied linear statistical models*. Irwin.

Newman, D. G., & Callister, R. (2008). Cardiovascular training effects in fighter pilots induced by occupational high G exposure. *Aviation Space and Environmental Medicine*, **79**(8), 774–778.

Newman, D. G., White, S. W., & Callister, R. (1998). Evidence of baroreflex adaptation to repetitive+ Gz in fighter pilots. *Aviation Space and Environmental Medicine*, **69**(5), 446–451.

Norsk, P. (2020). Adaptation of the cardiovascular system to weightlessness: Surprises, paradoxes and implications for deep space missions. *Acta Physiologica*, **228**(3), e13434.

Norsk, P., Damgaard, M., Petersen, L., Gybel, M., Pump, B., Gabrielsen, A., & Christensen, N. J. (2006). Vasorelaxation in space. *Hypertension*, **47**(1), 69–73.

Norsk, P., Foldager, N., Bonde-Petersen, F., Elmann-Larsen, B., & Johansen, T. S. (1987). Central venous pressure in humans during short periods of weightlessness. *Journal of Applied Physiology*, **63**(6), 2433–2437.

Ogawa, Y., Yanagida, R., Ueda, K., Aoki, K., & Iwasaki, K. (2016). The relationship between widespread changes in gravity and cerebral blood flow. *Environmental Health and Preventive Medicine*, **21**(4), 186–192.

Ogoh, S., Hirasawa, A., Raven, P. B., Rebuffat, T., Denise, P., Lericollais, R., Sugawara, J., & Normand, H. (2015). Effect of an acute increase in central blood volume on cerebral hemodynamics. *American Journal of Physiology-Regulatory, Integrative and Comparative Physiology*, **309**(8), R902–R911.

Petersen, L. G., Damgaard, M., Petersen, J. C. G., & Norsk, P. (2011). Mechanisms of increase in cardiac output during acute weightlessness in humans. *Journal of Applied Physiology*, **111**(2), 407–411.

Peterson, K., Ozawa, E. T., Pantalos, G. M., & Sharp, M. K. (2002). Numerical simulation of the influence of gravity and posture on cardiac performance. *Annals of Biomedical Engineering*, **30**(2), 247–259.

Pump, B., Videbæk, R., Gabrielsen, A., & Norsk, P. (1999). Arterial pressure in humans during weightlessness induced by parabolic flights. *Journal of Applied Physiology*, **87**(3), 928–932.

Saglietto, A., Tripoli, F., Zwanenburg, J., Biessels, G. J., De Ferrari, G. M., Anselmino, M., Ridolfi, L., & Scarsoglio, S. (2024). Role of the vessel morphology on the lenticulostriate arteries hemodynamics during atrial fibrillation: A CFD-based multivariate regression analysis. *Computer Methods and Programs in Biomedicine*, **254**, 108303.

Savarese, G., Stolfo, D., Sinagra, G., & Lund, L. H. (2022). Heart failure with mid-range or mildly reduced ejection fraction. *Nature Reviews Cardiology*, **19**(2), 100–116.

Saveko, A., Bekreneva, M., Ponomarev, I., Zelenskaya, I., Riabova, A., Shigueva, T., Kitov, V., Abu Sheli, N., Nosikova, I., Rukavishnikov, I., Sayenko, D., & Tomilovskaya, E. (2023). Impact of different ground-based microgravity models on human sensorimotor system. *Frontiers in Physiology*, **14**, 1085545.

Scarsoglio, S., Fois, M., & Ridolfi, L. (2023). Increased hemodynamic pulsatility in the cerebral microcirculation during parabolic flight-induced microgravity: A computational investigation. *Acta Astronautica*, **211**, 344–352.

Scarsoglio, S., Gallo, C., Saglietto, A., Ridolfi, L., & Anselmino, M. (2019). Impaired coronary blood flow at higher heart rates during atrial fibrillation: Investigation via multiscale modelling. *Computer Methods and Programs in Biomedicine*, **175**, 95–102.

Scott, J. M., Esch, B. T. A., Goodman, L. S., Bredin, S. S. D., Haykowsky, M. J., & Warburton, D. E. R. (2007). Cardiovascular consequences of high-performance aircraft maneuvers: Implications for effective countermeasures and laboratory-based simulations. *Applied Physiology, Nutrition, and Metabolism*, **32**(2), 332–339.

Shelhamer, M. (2016). Parabolic flight as a spaceflight analog. *Journal of Applied Physiology*, **120**(12), 1442–1448.

Shen, M., & Frishman, W. H. (2019). Effects of spaceflight on cardiovascular physiology and health. *Cardiology in Review*, **27**(3), 122–126.

Shender, B. S., Forster, E. M., Hrebien, L., Ryoo, H. C., & Cammarota, J. P. (2003). Acceleration-induced near-loss of consciousness: The "A-LOC" syndrome. *Aviation Space and Environmental Medicine*, **74**, 1021–1028.

Taibbi, G., Cromwell, R. L., Kapoor, K. G., Godley, B. F., & Vizzeri, G. (2013). The effect of microgravity on ocular structures and visual function: A review. *Survey of Ophthalmology*, **58**(2), 155–163.

Tanaka, K., Nishimura, N., & Kawai, Y. (2017). Adaptation to microgravity, deconditioning, and countermeasures. *The Journal of Physiological Sciences*, **67**(2), 271–281.

Traon, A. P.-L., Heer, M., Narici, M. V., Rittweger, J., & Vernikos, J. (2007). From space to Earth: Advances in human physiology from 20 years of bed rest studies (1986–2006). *European Journal of Applied Physiology*, **101**(2), 143–194.

Ueda, K., Ogawa, Y., Yanagida, R., Aoki, K., & Iwasaki, K. (2015). Dose-effect relationship between mild levels of hypergravity and autonomic circulatory regulation. *Aerospace medicine and human performance*, **86**(6), 535–540.

Videbaek, R., & Norsk, P. (1997). Atrial distension in humans during microgravity induced by parabolic flights. *Journal of Applied Physiology*, **83**(6), 1862–1866.

Westerhof, N., Stergiopulos, N., Noble, M. I. M., & Westerhof, B. E. (2019). *Snapshots of Hemodynamics*. Springer International Publishing. http://link.springer.com/10.1007/978-3–319-91932-4

Whittle, R. S., & Diaz-Artiles, A. (2021). Modeling individual differences in cardiovascular response to gravitational stress using a sensitivity analysis. *Journal of Applied Physiology*, **130**(6), 1983–2001.

Widjaja, D., Vandeput, S., Van Huffel, S., & Aubert, A. E. (2015). Cardiovascular autonomic adaptation in lunar and martian gravity during parabolic flight. *European Journal of Applied Physiology*, **115**(6), 1205–1218.

Young, L. R., & Sutton, J. P. (Eds.) (2021). *Handbook of Bioastronautics*. Springer International Publishing. https://link.springer.com/10.1007/978-3–319-12191-8

Zhang, L.-F., & Hargens, A. R. (2018). Spaceflight-induced intracranial hypertension and visual impairment: Pathophysiology and countermeasures. *Physiological Reviews*, **98**(1), 59–87.

Zhu, H., Wang, H., & Liu, Z. (2015). Effects of real and simulated weightlessness on the cardiac and peripheral vascular functions of humans: A review. *International Journal of Occupational Medicine and Environmental Health*, **28**(5), 793–802.

Additional information

Data availability statement

All model equations, parameter settings, code and generated raw simulation data are available on Figshare, along with the experimental data used for model validation (https://doi.org/10.6084/m9.figshare.29064842).

Competing interests

The authors declare that they have no competing interests that could appear to influence the work reported in this paper.

Author contributions

F.T., L.R., and S.S. conceived and designed the research, analyzed and interpreted the results, edited, and revised the manuscript. F.T. performed the numerical simulations. F.T. drafted the manuscript and prepared the figures. All authors reviewed and approved the final version of the manuscript. All authors agree to be accountable for all aspects of the work. All persons designated as authors qualify for authorship, and all those who qualify for authorship are listed.

Funding

This study was carried out within the I-2022-05387 'Optimizing countermeasures against cardiovascular deconditioning and cerebral haemodynamics changes in long-term human spaceflights' project, which was selected via the Open Space Innovation Platform (https://ideas.esa.int) as a Co-Sponsored Research Agreement and carried out under the Discovery programme of, and funded by, the European Space Agency (contract number: 4000141523). This manuscript reflects only the authors' views and opinions and the European Space Agency cannot be considered responsible for them.

Keywords

cardiac haemodynamics, cardiovascular modelling, hyper-gravity, micro-gravity, space medicine

Supporting information

Additional supporting information can be found online in the Supporting Information section at the end of the HTML view of the article. Supporting information files available:

Peer Review History